ELSEVIER

An overview of radar soundings of the martian ionosphere from the Mars Express spacecraft

D.A. Gurnett [a,*], R.L. Huff [a], D.D. Morgan [a], A.M. Persoon [a], T.F. Averkamp [a],
D.L. Kirchner [a], F. Duru [a], F. Akalin [a], A.J. Kopf [a], E. Nielsen [b],
A. Safaeinili [c], J.J. Plaut [c], G. Picardi [d]

[a] *Department of Physics and Astronomy, University of Iowa, Iowa City, IA 52242, USA*
[b] *Max Planck Institute for Solar System Research, 37191 Katlenburg-Lindau, Germany*
[c] *Jet Propulsion Laboratory, Pasadena, CA 91109, USA*
[d] *Infocom Department, "La Sapienza" University of Rome, 00184 Rome, Italy*

Abstract

The Mars Express spacecraft carries a low-frequency radar called MARSIS (Mars Advanced Radar for Subsurface and Ionosphere Sounding) that is designed to study the subsurface and ionosphere of Mars. In this paper, we give an overview of the ionospheric sounding results after approximately one year of operation in orbit around Mars. Several types of ionospheric echoes are commonly observed. These include vertical echoes caused by specular reflection from the horizontally stratified ionosphere; echoes from a second layer in the topside ionosphere, possibly associated with O^+ ions; oblique echoes from upward bulges in the ionosphere; and a variety of other echoes that are poorly understood. The vertical echoes provide electron density profiles that are in reasonable agreement with the Chapman photo-equilibrium model of planetary ionospheres. On the dayside of Mars the maximum electron density is approximately $2 \times 10^5 \, cm^{-3}$. On the nightside the echoes are often very diffuse and highly irregular, with maximum electron densities less than $10^4 \, cm^{-3}$. Surface reflections are sometimes observed in the same frequency range as the diffuse echoes, suggesting that small isolated holes exist in the nightside ionosphere, possibly similar to those that occur on the nightside of Venus. The oblique echoes arise from upward bulges in the ionosphere in regions where the crustal magnetic field of Mars is strong and nearly vertical. The bulges tend to be elongated in the horizontal direction and located in regions between oppositely directed arch-like structures in the crustal magnetic field. The nearly vertical magnetic field lines in the region between the arches are thought to connect into the solar wind, thereby allowing solar wind electrons to heat the lower levels of the ionosphere, with an attendant increase in the scale height and electron density.
© 2007 COSPAR. Published by Elsevier Ltd. All rights reserved.

Keywords: Mars ionosphere; Ionosphere radar sounding; Mars

1. Introduction

The Mars Express spacecraft, which was placed in an eccentric orbit around Mars on December 25, 2003, includes a low-frequency radar called MARSIS (Mars Advanced Radar for Subsurface and Ionosphere Sounding) that is designed to perform subsurface and ionosphere soundings. This paper gives an overview of the ionospheric sounding results after the first year of operation in orbit. The nominal orbit of Mars Express has a periapsis altitude of about 275 km, an apoapsis altitude of about 10,100 km, and an inclination of 86°. A typical MARSIS ionospheric sounding pass lasts about 40 min and starts at an altitude of 1200 km on the inbound leg, continues through periapsis, and ends at an altitude of 1200 km on the outbound

---

* Corresponding author.
E-mail address: donald-gurnett@uiowa.edu (D.A. Gurnett).

leg. Because of difficulties with the MARSIS antenna deployment, the instrument did not start operating until July 4, 2005. For a detailed description of the MARSIS instrument and its operation, see Picardi et al. (2004); and for a more detailed description of the Mars express spacecraft, see Chicarro et al. (2004).

Prior to the Mars Express mission, most of our knowledge of the Martian ionosphere came from radio occultation studies. This technique involves making accurate measurements of the phase shift produced as the telemetry signal from a spacecraft passes through the ionosphere. The phase shift provides a measurement of the average electron density along the line of sight. The first radio occultation measurements of the ionosphere of Mars were obtained from the Mariner 4 spacecraft, which flew by Mars in 1964 (Fjeldbo et al., 1966). Since then, extensive radio occultation measurements have been obtained from a variety of spacecraft in orbit around Mars, such as Viking 1 and 2, Mars Global Surveyor, and most recently by Mars Express. For radio occultation results from these and other spacecraft, see Zhang et al. (1990a,b), Luhmann and Brace (1991), Kliore (1992), Mendillo et al. (2004), and Pätzold et al. (2005). Because of geometric considerations involving the orbits of Earth and Mars, occultations can only be obtained at solar zenith angles from about 44° to 136°. As we will show the MARSIS ionospheric soundings nicely complement these radio occultation measurements by providing improved horizontal spatial resolution and the ability to make observations at solar zenith angles where radio occultations cannot be obtained.

The only direct in situ measurements of the Martian ionosphere are from retarding potential analyzers on the Viking 1 and 2 landers, which descended through the ionosphere of Mars on July 20 and September 3, 1976 (Hanson et al., 1977). These measurements showed that the peak electron density is about 10^5 cm^{-3} at an altitude of about 125–135 km, and that the dominant ion is O_2^+. Smaller concentrations of CO_2^+ and O^+ were also observed. Scale heights inferred from the density profiles were about 20–30 km, and typical electron temperatures were found to be 2000–4000 K (Hanson and Mantas, 1988). The Viking data also showed that the solar wind provides an important energy source in the upper levels of the ionosphere, and that the plasma pressure in the ionosphere is less than the average solar wind dynamic pressure (Hanson and Mantas, 1988; Luhmann and Brace, 1991). It was estimated that a magnetic field of about 30–40 nT is required in the ionosphere to provide pressure balance on the dayside of Mars. Although Mars has no intrinsic large-scale magnetic field, later measurements from the Mars Global Surveyor (MGS) spacecraft showed that Mars has significant small-scale crustal magnetic fields, with peak field strengths at 100 km sometimes as high as 1600 nT (Acuña et al., 1998, 1999). As we will show, crustal magnetic fields play an important role in controlling small-scale structures in the Martian ionosphere.

2. Principles of ionospheric sounding

Spacecraft-borne ionospheric sounders were initially developed in the 1960s to study the topside of Earth's ionosphere (Calvert, 1966; Franklin and Maclean, 1969; Hagg et al., 1969). Ionospheric sounders operate by transmitting a short pulse at a fixed frequency, f, and then detecting any echoes that are reflected from the ionosphere. Reflection occurs because free-space electromagnetic radiation cannot propagate at frequencies below the electron plasma frequency, which is given by $f_p = 8980\sqrt{n_e}$ Hz, where n_e is the electron number density in cm^{-3} (Gurnett and Bhattacharjee, 2005). For normal incidence on a horizontally stratified ionosphere, reflection occurs at the altitude where the plasma frequency is equal to the wave frequency, i.e., $f_p = f$. By measuring the time delay, Δt, between the transmission of the pulse and the time that the echo is received, the range to the reflection point can be computed. The basic geometry is illustrated in the top panel of Fig. 1, which shows a representative plot of the plasma frequency as a function of altitude, $f_p(z)$, in the Martian ionosphere. By sequentially stepping the transmitter frequency after each transmit-receive cycle, the time delay, and hence the range to the reflection point, can be determined as a function of frequency. A plot of the time delay as a function of frequency, $\Delta t(f)$, can then be made, as illustrated in the
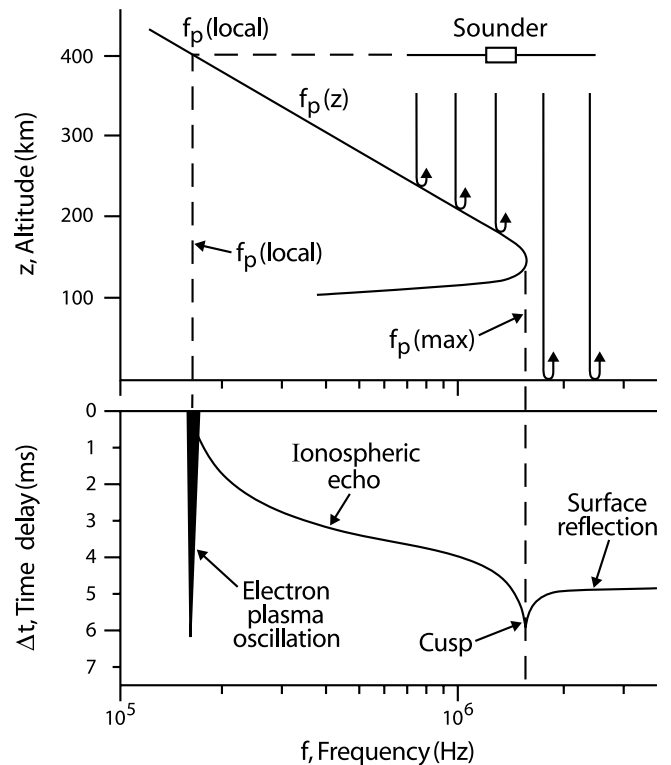

Fig. 1. The top panel shows a representative profile of the electron plasma frequency, f_p, in the Martian ionosphere, and the bottom panel shows the corresponding ionogram, which is a plot of the time delay, Δt, for a sounder pulse of frequency, f, to reflect from the ionosphere and return to the spacecraft.

bottom panel of Fig. 1. This type of plot is called an iono-gram. Although a rough estimate of the time delay to the reflection point can be obtained by assuming that the pulse travels at the speed of light, c, for accurate computations the effect of the plasma on the propagation velocity of the pulse must be considered. This effect is called dispersion. It is well known that the propagation velocity of a pulse in an unmagnetized plasma is given by $v_g = c\sqrt{1 - (f_p/f)^2}$. This velocity is called the group velocity. The round-trip time delay for vertical incidence on a horizontally stratified ionosphere is then given by

$$\Delta t(f) = \frac{2}{c} \int_{z(f_p)}^{z_{sc}} \frac{dz}{\sqrt{1 - (f_p(z)/f)^2}}, \tag{1}$$

where the integration is carried out from the altitude of the reflection point, $z(f_p)$, to the altitude of the spacecraft, z_{sc}.

An ionogram usually has certain characteristic features. As the transmitter steps upward in frequency the first response detected is a strong, long lasting echo when the frequency reaches the local plasma frequency, $f_p(local)$. This response is caused by the excitation of electrostatic electron plasma oscillations at the local electron plasma frequency and produces the vertical spike labeled "electron plasma oscillation" in the bottom panel of Fig. 1. As soon as the transmitter frequency exceeds the local plasma frequency, electromagnetic wave propagation can start to occur. Remote echoes from the ionosphere can then be detected, starting initially at zero time delay, and then with a steadily increasing time delay as the range to the reflection point increases. These echoes produce the trace labeled "ionospheric echo" in Fig. 1. As the transmitter frequency approaches the maximum plasma frequency in the iono-sphere, $f_p(max)$, the time delay increases rapidly, forming the left-hand branch of the feature labeled "cusp". The cusp occurs because the group velocity goes to zero over a rapidly increasing path length as the frequency approaches $f_p(max)$. As soon as the transmitter frequency exceeds $f_p(max)$ the pulse can pass through the ionosphere to the surface of the planet, where it reflects and returns to the spacecraft, forming the right-hand branch of the cusp.

By measuring the time delay as a function of frequency, the function $\Delta t(f)$ on the left-hand side of Eq. (1) can be determined. To obtain the electron density as a function of altitude, the problem is then to solve for the function $f_p(z)$ inside the integral. The solution of this integral equation, called Abel's equation, is a classical problem in mathematical physics (Whittaker and Watson, 1927), and has a formal solution (Budden, 1961) given by

$$z(f_p) = \frac{2}{\pi} \int_{\alpha_0}^{\pi/2} c\Delta t(f_p \sin \alpha) d\alpha, \tag{2}$$

where $\sin \alpha = f_p(z)/f$ and $\sin \alpha_0 = f_p(z_{sc})/f_p(max)$. Since time delay measurements must be made at a discrete set of frequencies, to apply this equation the integral must be converted to a discrete sum of integrals. The integration

for any arbitrary frequency f is then equivalent to dividing the ionosphere into a series of horizontal slabs extending from the spacecraft, i.e., where $\alpha = \alpha_0$, to the point where the plasma frequency is equal to the wave frequency, i.e., where $\alpha = \pi/2$.

3. Electron density profiles

During the mode of operation normally used by MAR-SIS for ionospheric sounding, the transmitter steps through 160 quasi-logarithmically spaced frequencies ($\Delta f/f \approx 2\%$) from 0.1 to 5.4 MHz. A complete sweep takes 1.257 s, and the sweep cycle is repeated once every 7.54 s. At each frequency step a 91.4 μs quasi-sinusoidal pulse is transmitted and the resulting echo intensities are recorded in 80 equally spaced time delay bins from 0 to 7.31 ms. The echo intensities received during each frequency sweep are displayed in the form of a color-coded ionogram, such as the one shown in Fig. 2. The closely spaced vertical lines near the left edge of the ionogram are at the harmonics of the local electron plasma frequency and are caused by the excitation of electrostatic electron plasma oscillations at the local electron plasma frequency. The harmonics are caused by nonlinear distortion in the receiver. In this case the plasma frequency is below the 0.1 MHz low-frequency cutoff of the receiver, and cannot be detected directly. However, the plasma frequency can be determined from the harmonic spacing and is $f_p(local) = 0.09$ MHz. At somewhat higher frequencies a very strong ionospheric echo trace can be seen extending from about 0.6 to 2 MHz, with time delays ranging from about 2.5 to 3.5 ms. The echo trace ends in a well-defined cusp at
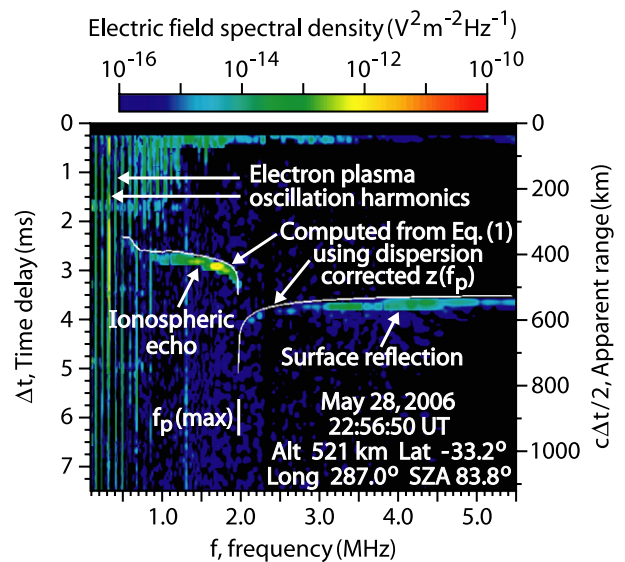

Fig. 2. A color-coded ionogram showing the echo intensity as a function of the time delay, Δt, and frequency, f. To provide a rough estimate of the range to the reflection point, the scale on the right gives the apparent range, which is defined as $c\Delta t/2$, where c is the speed of light. The white line shows the time delay computed from Eq. (1) using the dispersion-corrected plasma frequency profile shown in Fig. 3.

1.98 MHz, which from the discussion in the previous section allows us to make an accurate determination of the maximum plasma frequency in the ionosphere, $f_p(\max) = 1.98$ MHz. At frequencies above 1.98 MHz, a weak but easily detectable surface reflection can be detected. This reflection becomes progressively more intense and better defined as the frequency increases toward the upper limit of the sweep. The intensity of the surface reflection in this case is relatively strong. However, the surface reflection varies considerably from pass to pass, and sometimes disappears completely during periods of intense solar activity due to enhanced absorption near and below the peak in the density profile. For a discussion of the solar control of the surface reflections detected by MARSIS, see Morgan et al. (2006).

Next, we show how the ionospheric echo trace can be converted to an electron density profile. The first step is to scale the time delay as a function of frequency from the ionogram. The leading edge of the echo is used for this scaling because our convention is to measure the delay time from the start of the transmitter pulse. In principle, once the time delays have been scaled from the ionogram, the dispersion-corrected altitudes, $z(f_p)$, can be computed directly from Eq. (2). However, in this, as in most cases, the echo intensity at the low-frequency end of the sweep is too weak to allow continuous measurements down to the local plasma frequency. Therefore, we must make a reasonable guess as to how the trace extends across the gap from the local plasma frequency (0.09 MHz) to the lowest frequency for which the time delay can be measured (0.6 MHz). To interpolate through this gap we assume that the plasma frequency profile varies exponentially with altitude, with the parameters adjusted so that the profile matches the known values at the end points. This procedure gives the plasma frequency profile shown by the black line and the black dots marked "dispersion-corrected altitudes" in Fig. 3. The corresponding electron densities are shown by the scale at the top of the plot. It should be noted that, since the echo trace only involves reflections from the topside of the ionosphere, these echoes can provide no information on the electron density profile on the bottomside of the ionosphere, such as can be obtained from radio occultation measurements. However, for the topside ionosphere, the sounder can provide information on electron densities as low as 1.24×10^2 cm^{-3} (corresponding to a plasma frequency of $f_p = 0.1$ MHz), which is considerably lower than can be obtained from radio occultation measurements.

As a check on the overall accuracy of the inversion process, we next use the dispersion-corrected plasma frequency profile to compute the time delay as a function of frequency using Eq. (1), and then compare this result with the measured time delays. The time delay computed from the plasma frequency profile in Fig. 3 is shown by the white line in Fig. 2. As can be seen, the agreement with the observed time delay is very good, including the surface reflection, which was not used in the inversion procedure.
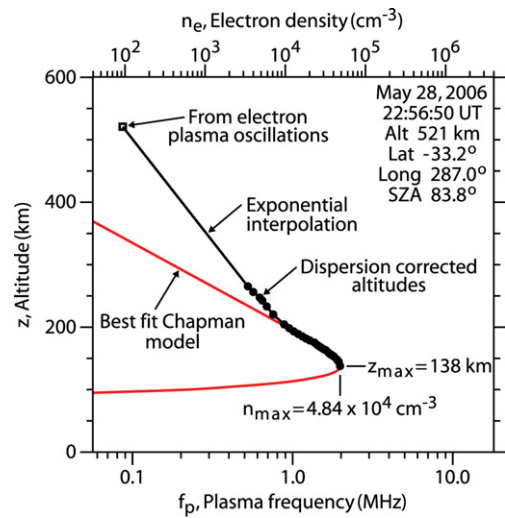

Fig. 3. The black dots show the dispersion-corrected altitudes computed from the measured time delays of the ionospheric echo trace in Fig. 2, and the open square shows the plasma frequency at the spacecraft as obtained from the frequency of locally excited electron plasma oscillations. The solid black line shows the plasma frequency profile, including the exponential interpolation across the large gap between the local plasma frequency (0.09 MHz) and the lowest frequency for which a remote echo was detected (0.6 MHz). This plasma frequency profile was used to compute the white line in Fig. 2. The red line is the best fit to the Chapman (1931) electron density model.

Although it is in principle possible to construct the bottomside electron density profile from a combined analysis of both the ionospheric echo trace and the surface reflection trace, in practice the accuracy is not good enough to provide a reconstruction of the bottomside profile. The main information that can be obtained from the surface reflection is the total electron content (TEC) integrated through the ionosphere. In this case the best fit to the dispersion of the surface reflection gives $TEC = 3.06 \times 10^{11}$ cm^{-2}, which is a typical value at this solar zenith angle (83.8°). The solar zenith angle (SZA) is the angle between the direction to the Sun and the local vertical.

Having computed the dispersion-corrected plasma frequency profile we next compare the electron densities (given at the top of Fig. 3) with the well-known Chapman (1931) photo-equilibrium theory of planetary ionospheres. The electron density in Chapman's model is given by

$$n_e = n_0 \exp\left[\frac{1}{2}\left\{1 - \frac{z - z_0}{H} - \text{Ch}(\text{x},\chi)\exp\left(-\frac{z - z_0}{H}\right)\right\}\right], \qquad (3)$$

where n_0 is the maximum electron density at the subsolar point, z_0 is the altitude of this maximum, and $\text{Ch}(\text{x}, \chi)$ is a function called the Chapman grazing incidence function. The grazing incidence function takes into account the absorption of the solar radiation as it passes obliquely through the ionosphere, and can be computed from a power series provided by Chapman. The grazing incidence function depends on the solar zenith angle χ and a dimen-

sionless parameter $x = (R_M + z_0)/H$, where $R_M = 3396$ km is the radius of Mars, and H is the scale height of the neutral atmosphere. The red line in Fig. 3 shows the best least-squares fit of Eq. (3) to the first 16 points below the peak in the dispersion-corrected electron density profile. The fitting procedure is terminated just before the well-defined break in the profile at about 1 MHz. This break is thought to mark the transition between the photo-equilibrium dominated region at low altitudes, and the transport dominated region at high altitudes (Fox, 1997). The best fit parameters for the Chapman fit are $n_0 = 1.32 \times 10^5$ cm^{-3}, $z_0 = 107$ km, and $H = 15.2$ km. Note that n_0 and z_0 refer to the subsolar point. At the location where the measurements were made (SZA = 83.8°) the maximum electron density is $n_{max} = 4.84 \times 10^4$ cm^{-3} and the altitude of the maximum is $z_{max} = 138$ km. When compared to electron density profiles obtained from radio occultation measurements at a comparable solar zenith angle (Mendillo et al., 2004) these parameters appear to be very reasonable. However, at the subsolar point the density, n_0, and the altitude of the maximum, z_0, are both too small, indicating that Chapman's model does not provide satisfactory results when extrapolated to solar zenith angles far removed from where the sounding was made. For a discussion of various factors that can lead to deviations from the Chapman model, especially at solar zenith angles near the terminator, see Fox and Yeager (2006).

Although the Chapman model fits the locally measured electron density profile very well, the parameters are somewhat sensitive to the profile used to interpolate across the gap between the local plasma frequency and the lowest frequency at which the ionospheric echo trace can be measured. For example, if for the event in Fig. 2 we change from an exponential to a linear interpolation to carry out the inversion the parameter z_{max} increases from 138 to 148 km, and the scale height H increases from 15.2 to 23.8 km. We have tried a number of other functions that match the end points, and also functions that match the slope of the lowest few dispersion-corrected altitudes. All give similar, but slightly different results. Since the simple exponential interpolation used in Fig. 3 appears to connect smoothly with the dispersion-corrected altitudes, we believe that this is probably the most reasonable choice. It is worth pointing out that although z_{max} and H are somewhat sensitive to the choice of the interpolation function, the parameter n_{max} is almost completely insensitive to this choice. This parameter depends mainly on the frequency of apex of the cusp, i.e., f_p(local), and can usually be measured very accurately.

Although most of the ionospheric echo traces follow the shape predicted by the Chapman model near the nose of the profile, there are often significant deviations from the Chapman model at higher altitudes, above about 200 km. These deviations in some case involve a smooth increase that indicates the onset of a vertical transport process, as in Fig. 3, and in other cases involve a discontinuous change in slope that suggests the presence of a second layer in the
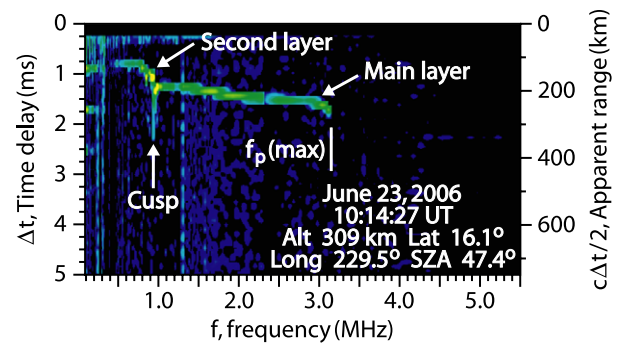

Fig. 4. An ionospheric echo that shows a clearly defined cusp at about 0.9 MHz, well below the cusp at 3.2 MHz associated with the main layer of the ionosphere. The cusp at 0.9 MHz indicates the presence of a second layer in the topside of the ionosphere at an altitude of about 200 km.

topside ionosphere. An ionogram that provides strong evidence for the existence of a second layer is shown in Fig. 4. As can be seen, a well-defined cusp occurs in the ionospheric echo trace at a frequency of about 0.9 MHz, which is well below the main peak in the plasma frequency profile at about 3.2 MHz. As discussed in the earlier section on the principles of ionospheric sounding, the formation of a cusp in the echo trace indicates a local maximum in the electron density profile, i.e., a region in the profile where $df_p/dz = 0$. From the apparent range of this echo, which is about 100 km, and from the altitude of the spacecraft, which is 309 km, we estimate that the altitude of the second layer is about 200 km. Although ionograms with a well-defined cusp in the topside ionosphere, such as in Fig. 4, are not very common, the occurrence of a discontinuous change in the slope of the time delay trace at about 200 km is quite common. Comparisons with the Viking 1 and 2 data of Hanson et al. (1977) suggest that this second layer may be due to O$^+$ ions. Transport effects caused by the interaction of the solar wind with the ionosphere, such as modeled by Ma et al. (2004), may act to enhance the O$^+$ peak in the electron density profile. Magnetic field effects may also be important. In studies of the Venusian ionosphere, Shinagawa et al. (1991) have found that a second peak in the topside ionosphere can occur if the ionosphere is magnetized. Further studies are being planned to investigate the properties of this second layer and its relationship to the various transport and magnetic field effects that are known to occur in the Martian ionosphere.

4. Solar zenith angle dependence

Because of gravitational perturbations, the Mars Express orbit evolves rather rapidly. During the first year of operation nearly complete data coverage was obtained for solar zenith angles ranging from nearly 0° to 180°. This good coverage allows us to carry out a detailed examination of the solar zenith angle dependence that is implicit in Eq. (3). It is easy to show from Chapman's theory that the maximum electron density at the peak of the profile is given by

$$n_e(\mathrm{max}) = (q_0/\alpha)^{1/2}/\mathrm{Ch}(x,\chi)^{1/2}, \qquad (4)$$

where q_0 is the ionization rate at the subsolar point and α is the recombination rate. In principle, $n_e(\mathrm{max})$ can be determined for every sounding sweep by measuring the maximum frequency, $f_p(\mathrm{max})$, of the ionospheric echo trace. In Fig. 5 we show a plot of the maximum frequency of the ionospheric echo, $f_p(\mathrm{max})$, as a function of solar zenith angle, χ. This plot includes over 8000 data points from 71 orbits extending over the period from August 4, 2005, to May 28, 2006. The solar F10.7 index, which is often used as a proxy for the solar EUV radiation that causes the ionization, was generally decreasing during this period, varying from 119 to 72, with a mean of 84. Sometimes the maximum frequencies of the ionospheric echoes do not extend to a well-defined cusp due to absorption near the peak in the plasma frequency profile. Therefore, the frequencies given in this plot are rigorously only a lower limit to the maximum plasma frequency. However, since the absorption is mainly confined to the region near and below the maximum, in most cases we believe that the maximum echo frequency is very close to $f_p(\mathrm{max})$. For comparison a plot of $n_e(\mathrm{max})$ computed from Eq. (4) is shown by the red line labeled "Best-fit Chapman model". The parameter $(q_0/\alpha)^{1/2} = 1.98 \times 10^5\ \mathrm{cm}^{-3}$ has been selected so that the red line lies near the upper limit of the most dense cluster of points which, given the above considerations, is our best estimate of $f_p(\mathrm{max})$. As can be seen the red line closely follows the basic solar zenith angle dependence exhibited in most of the data.

Although Chapman's model provides a reasonably good fit to most of the data in Fig. 5, there are isolated events that have maximum echo frequencies both well below and well above the dense cluster of points that are charac-

teristic of the Chapman curve. The ones that extend well below the dense cluster of points are generally cases where the echo intensity is very weak, so that the echo trace disappears well before reaching $f_p(\mathrm{max})$. The cause of the low intensities in these cases is at present poorly understood. The relatively few points that are well above the dense cluster of points may look like they might be due to some type of data error, but they are not. Some of these have ready explanations, and others do not. For example, the density enhancement represented by the series of data points labeled "Class X1.1 solar flare" can be attributed to a very intense solar flare that occurred at 08:30 UT (Universal Time) on September 15, 2005. Evidently, energetic solar radiation from this flare caused an increase in the ionization rate, q_0 in Eq. (4), with an attendant increase in the electron density. Other outlying points are more difficult to understand. A good example is Event A in the upper left-hand corner of the plot. The ionogram of this event is shown in Fig. 6. As can be seen, a clear ionospheric echo can be detected extending up to a frequency of about 5.1 MHz, one of the highest plasma frequencies ever observed. Although not shown, this is just one of a series of ionograms with similar echoes obtained in this same region extending over a period of about 30 s. We have checked the solar activity records for this period, and there is no evidence of a solar flare or any other solar activity that can be associated with this event. Also, investigation of the ASPERA plasma data on Mars Express revealed no evidence of energetic particles that could account for the enhanced electron densities. The one relationship we have noted is that during this time the spacecraft was passing over a region with an exceptionally strong crustal magnetic field, approximately 200 nT at the spacecraft, which is at an altitude of 294 km. We believe that the sounder may
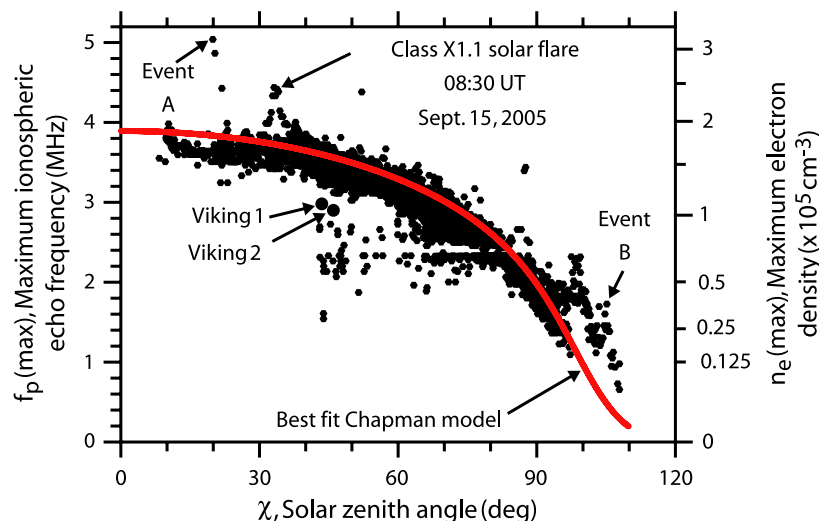

Fig. 5. A plot of the maximum ionospheric echo frequency as a function of solar zenith angle for all of the ionograms processed during the first year of operation. The red line is the maximum plasma frequency predicted by the Chapman (1931) electron density model. Since the maximum echo frequency sometimes does not extend to the cusp at $f_p(\mathrm{max})$, the $(q_0/\alpha)^{1/2}$ parameter in Eq. (4) has been adjusted so that the curve is near the upper limit of the most dense cluster of points.
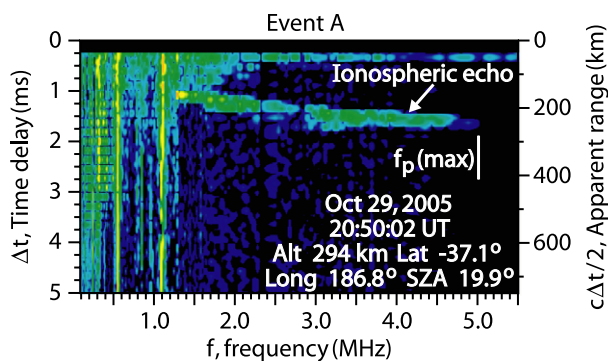
Fig. 6. An ionogram of "Event A" in Fig. 5 near the subsolar point. The ionospheric echo in this case has an unusually large maximum plasma frequency, much larger than any of the others in this region. This event occurs in a region with a very strong crustal magnetic field.

Fig. 7. An ionogram of "Event B" in Fig. 5 on the nightside of Mars. The ionospheric echo in this case is very diffuse and overlaps the echo from the surface reflection. Such an overlap is impossible for a horizontally stratified ionosphere and suggests the presence of localized holes in the ionosphere that allow the transmitted signal to pass through the ionosphere and return to the spacecraft.

be detecting a region of dense plasma trapped in a mini-magnetosphere (Krymskii et al., 2003), or in a cusp-like magnetic field configuration that is exposed to the incident solar wind. Further investigation is needed to understand the origin of this unusual event.

Another region where the electron densities extend well above those predicted by the Chapman model is on the nightside of Mars. As can be seen in Fig. 5, for solar zenith angles greater than about 90° the electron densities are highly irregular and extend well above the densities predicted by Chapman's model. The ionospheric echoes in this region are often very diffuse and tend to occur in highly localized regions. An example of such a diffuse echo is shown in Fig. 7, which corresponds to the point marked "Event B" in the lower right-hand corner of Fig. 5. As can be seen the ionospheric echo in this case is diffuse and poorly defined, somewhat reminiscent of the "spread F" echoes that are observed from the F region of the terrestrial ionosphere (Wright et al., 1996). In this case the diffuse echoes were detected over a period of a little more than 2 min, corresponding to a horizontal distance of about 400 km. The diffuse nature of these echoes suggests that the radar pulse is being scattered by highly irregular structures in the ionosphere, possibly over a range of incidence angles, which would account for the spread in time delays. Also, note in Fig. 7 that the minimum frequency of the surface reflection, ~1.2 MHz, extends well below the maximum frequency of the diffuse ionospheric echo, ~1.9 MHz. Such a condition is impossible for a horizontally stratified ionosphere, and strongly suggests that the ionosphere is highly structured, possibly with holes similar to those observed on the nightside of Venus (Brace et al., 1983). Because of the variable and limited spatial extent of events such as in Fig. 7, we suspect that the enhanced electron densities associated with these echoes may be produced by low-energy auroral electrons precipitating into the atmosphere, such as those recently reported by Brain et al. (2006) and Lundin et al. (2006). Also, Ma et al. (2004) have pointed out that the dayside interaction of the ionosphere with the solar wind can cause a substantial
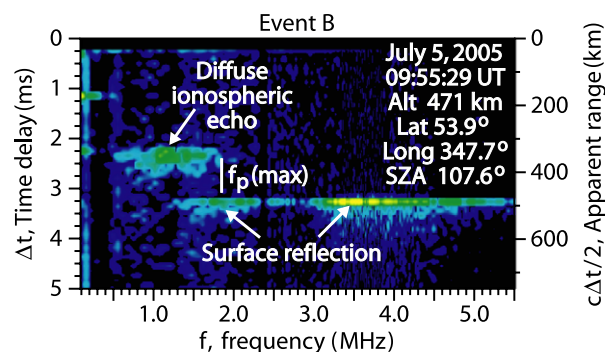
transport of ions from the dayside to the nightside, thereby causing unusual effects that otherwise would not be expected from Chapman's model.

5. Oblique ionospheric echoes

Double and sometimes multiple ionospheric echoes are a common feature of the MARSIS ionospheric soundings on the dayside of Mars. A good example is given by the ionogram in Fig. 8 which shows a double ionospheric echo observed at an altitude of 879 km and a solar zenith angle of 64.8°. In an earlier report, Gurnett et al. (2005) showed that when such multiple echoes occur, the echo with the shortest time delay originates from a vertical reflection from the ionosphere, and that the echoes with longer time delays originate from oblique reflections from fixed targets in the ionosphere. A good way to demonstrate this relationship is to display the time delays of the echoes in the form of a radargram, which is a plot of the echo intensity at a fixed frequency as a function of time and apparent altitude. Apparent altitude is defined as the spacecraft altitude minus the apparent range. A radargram for the entire pass in which the ionogram in Fig. 8 was obtained is shown in Fig. 9. In this case the frequency range, 2.0–3.0 MHz, was chosen so that both echoes can be detected. As can be seen, the echo with the shortest time delay, labeled "vertical ionospheric echo", remains at a nearly constant apparent altitude of about 150 km during the entire pass, consistent with a vertical reflection from the main horizontally stratified layer of the ionosphere. In sharp contrast, the apparent altitude of the echo with the longer time delay, labeled "oblique ionospheric echo", starts at about −140 km (which is impossible for a vertical echo) and increases rapidly until it merges with the main ionospheric echo at about 06:21 UT. The fact that the apparent altitude of this second echo is below the main horizontal layer of the ionosphere is a strong indication that this echo must be an oblique reflection from some distant feature in the
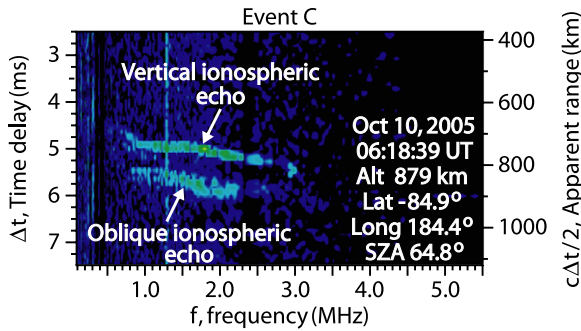
Fig. 8. An example of a double ionospheric echo observed on the dayside of Mars at a solar zenith angle of 64.8°. The echo with the shortest time delay is the vertical echo from the main horizontally stratified layer of the ionosphere, and the echo with the longer time delay is an oblique echo that originates from a small structure in the ionosphere that is fixed with respect to Mars.
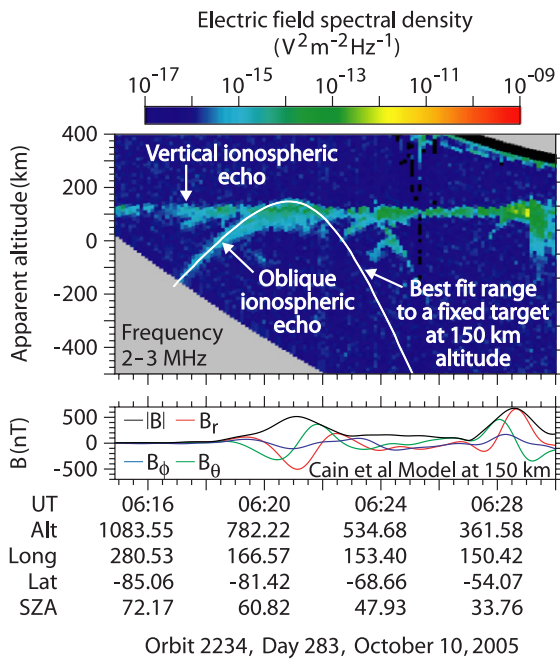

Fig. 9. A radargram showing the apparent altitude (defined as the spacecraft altitude minus the apparent altitude) as a function of time for the entire pass in which the ionogram in Fig. 8 was obtained. The vertical echo from the main horizontally stratified layer of the ionosphere corresponds to the horizontal line at an apparent altitude of about 150 km. The oblique echo corresponds to the hyperbola-shaped trace that starts at about 06:17 UT at an altitude of minus 140 km and merges with the main ionospheric echo at about 06:21 UT. The white hyperbola-shaped line is the best fit to the oblique echo trace computed assuming that the echo originates from a small fixed target located at an altitude of 150 km in the ionosphere immediately below the spacecraft at a time (06:20:55 UT) selected to give the best fit.

ionosphere. That the second echo is indeed consistent with an oblique reflection is shown by the hyperbola-shaped white line in Fig. 9. This line shows the apparent altitude calculated for reflection from a fixed point target in the ionosphere. The best fit is obtained if the target is at an altitude of 150 km and located at the latitude and longitude where the two echoes merge (06:20:55 UT). As can be seen,

the fit of the white line to the echo trace is very good, thereby providing strong confirmation that the echo is an oblique reflection from some small isolated feature in the ionosphere. Gurnett et al. (2005) also showed that oblique echoes of this type originate from regions where the crustal magnetic field is strong and nearly vertical. This relationship is illustrated in the bottom panel of Fig. 9, which shows the radial (B_r), southward (B_θ) and eastward (B_ϕ) components of the magnetic field, and the magnitude (B) of the magnetic field computed at an altitude of 150 km using the global magnetic field model developed by Cain et al. (2003). As can be seen, the apex of the hyperbola-shaped echo trace coincides with a region where the crustal magnetic field is both strong and nearly vertical.

Oblique echoes with hyperbola-shaped radargram traces, similar to the one illustrated in Fig. 9, are a very common feature in the MARSIS data. The hyperbola-shaped trace can appear either as a full hyperbola, or as a partial hyperbola branching either to the right or to the left with about equal probability (Duru et al., 2006). Usually the apex of the hyperbola is located near a region with a strong vertical magnetic field, as in Fig. 9. Evidence for this relationship is given in Fig. 10, which shows the results of a study of 211 clearly defined hyperbola-shaped echo traces of the type shown in Fig. 9. This plot shows the number of events as a function of the angle between the magnetic field and the local vertical evaluated at the apexes of the hyperbola-shaped echo traces. As can be seen, the number of events is strongly concentrated at small angles, less than about 30°. The basic picture that emerges from these studies is that the oblique echoes originate from an upward bulge in the ionosphere that is located in a region where the crustal magnetic field is nearly vertical, such as illustrated in Fig. 11. This picture is consistent with previous radio occultation studies showing that the plasma scale height in the Martian ionosphere increases in regions where the crustal magnetic field is nearly vertical (Ness et al., 2000; Mitchell et al., 2001; Krymskii et al., 2003, 2004). The increase in the plasma scale height is believed to be due to heating of the ionospheric electrons by solar wind
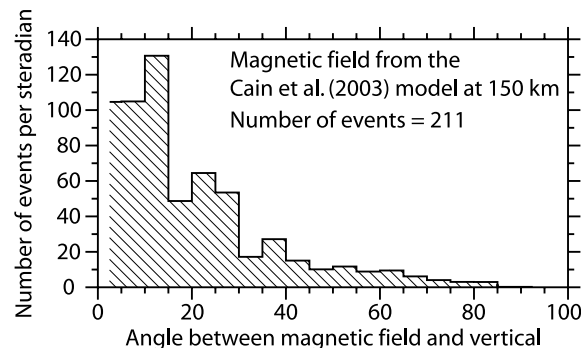

Fig. 10. A plot of the number of oblique echoes as a function of the angle between the magnetic field and the local vertical evaluated at the apex of 211 clearly defined hyperbola-shaped echo events similar to the one shown in Fig. 9.
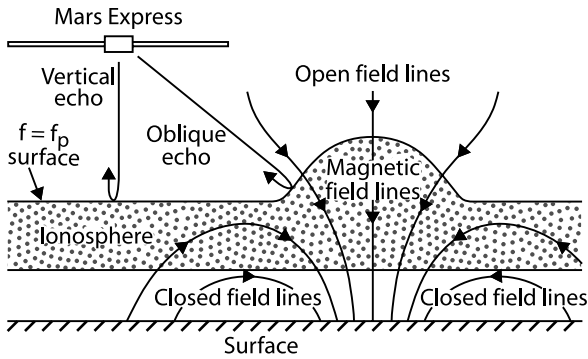
Fig. 11. The geometry of the ionospheric density structures that are thought to be responsible for oblique ionospheric echoes. As the spacecraft approaches the bulge in the ionosphere the sounder detects two echoes, a vertical echo from the horizontally stratified ionosphere, and an oblique echo from the bulge. The bulges are usually located between oppositely directed arch-like structures in the crustal magnetic field, in regions where the magnetic field is nearly vertical.

electrons that have access to the lower levels of the ionosphere along the nearly vertical (open) magnetic field lines.

Because of the close relationship between the ionospheric density bulges and the crustal magnetic field, it is of interest to investigate how the geometry of the density bulges relates to the geometry of the crustal magnetic fields. Inspections of many radargrams, such as Fig. 9, show that the apexes of the hyperbola-shaped echoes in almost all cases either merge with, or slightly overshoot, the echo trace associated with the surrounding horizontally stratified ionosphere. Evidence supporting this observation is given in Fig. 12, which shows the distribution of the number of events as a function of Δh, which is the difference of the apparent altitude at the apex of the hyperbola-shaped
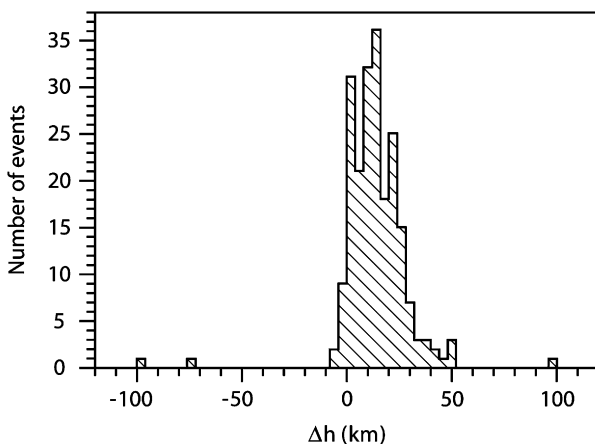

Fig. 12. A plot of the number of events (using the same data as in Fig. 10) as a function of the difference, Δh, between the apparent altitude at the apex of the hyperbola and the apparent altitude of the surrounding horizontally stratified ionosphere. Note the near absence of events with Δh less than zero, indicating that at closest approach the reflection is almost always from directly below the spacecraft. Such a distribution can only occur from horizontally elongated structures, and is inconsistent with reflections from a random horizontal distribution of small hemispherical structures.

trace and the apparent altitude of the surrounding ionosphere, for the same 211 events described earlier. The root-mean-square value of Δh (relative to zero) is 16 km, and the upper limit of the main part of the distribution is approximately 50 km. Since the spacecraft is usually at an altitude of several hundred kilometers or more, the bulges are small compared to the typical range to the spacecraft. This explains why the oblique echoes can be modeled by assuming that they originate from a small localized target. However, the amplitudes are not small when compared to the scale height of the ionosphere, which is typically about 10–15 km. Therefore, the bulges are a major feature in the Martian ionosphere. Also, note that there are almost no negative Δh values. This means that the bulges consist of horizontally elongated (half-cylindrical-shaped) structures, rather than hemispherical structures. For reflection from a horizontal cylinder, it is easily verified that the normal incidence point is always located directly below the spacecraft at closest approach, so Δh is never negative. In general, this is not the case for a random horizontal distribution of small hemispherical reflectors.

Finally we conclude this study of oblique reflection by comparing the locations of the ionospheric bulges detected by MARSIS with a color-coded map of the crustal magnetic field produced by Connerney et al. (2005). This map is shown in Fig. 13. As discussed by Connerney et al., the color-coded quantity, $\Delta B_r/\Delta Lat$, shown in this map is a proxy for the southward component of the magnetic field, $-B_\theta$. Thus, the red-shaded regions tend to have a northward directed field, and the blue-shaded regions tend to have a southward directed field. The black dots in Fig. 13 show the locations of the 211 oblique echo events described earlier, as determined from the apexes of the hyperbola-shaped echoes. As one can see, the black dots have a very strong tendency to occur at the boundaries between the blue- and red-coded regions. It is along these boundaries that the magnetic field is nearly vertical. Note the strong tendency for the blue- and red-coded regions to be elongated in the east-west direction. The magnetic field lines in a vertical north-south cut through blue-red regions would then have oppositely directed arch-like structure such as shown in Fig. 11. Given the strong tendency for the crustal magnetic field to have horizontally elongated arch-like structures of alternating polarities, called ''magnetic cylinders'' by Mitchell et al. (2001), it is not surprising that the ionospheric density bulges, which occur between these magnetic cylinders, would also consist of horizontally elongated cylindrical structures.

6. Electron cyclotron echoes

In addition to the vertical and oblique ionospheric echoes, many of the MARSIS ionospheric soundings display a series of echoes, equally space in time, at frequencies below about 1 MHz. These echoes typically appear as a series of horizontal bars along the left-hand side of an ionogram, such as in Fig. 14. Comparisons of the time delay between
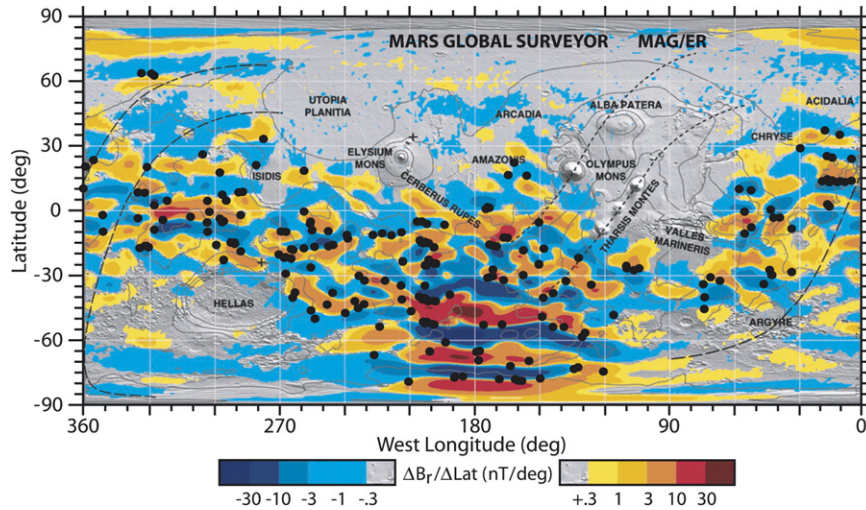
Fig. 13. The black dots show the locations of the apexes of the 211 hyperbola-shaped oblique echo events plotted on a map of the Mars crustal magnetic field prepared by Connerney et al. (copyright 2005, National Academy of Sciences, USA). Note that the black dots tend to occur near the boundaries between the blue and red regions. The magnetic fields in the red and blue regions have oppositely directed cylindrical arch-like structures of the type shown in Fig. 11.

these echoes, T_c, with the magnetic field model of Cain et al. (2003) shows that the repetition rate of these echoes, $1/T_c$, is almost exactly the local electron cyclotron frequency, $f_c = 28\,B$ Hz, where B is the magnetic field strength in nT. Because of the close association with the electron cyclotron frequency, Gurnett et al. (2005) called these echoes "electron cyclotron echoes." Echoes near the electron cyclotron frequency and its harmonics are a common feature of terrestrial ionospheric soundings and are usually attributed to the excitation of Bernstein mode waves (Hagg et al., 1969), which are electrostatic waves that occur between harmonics of the electron cyclotron frequency. Although the electron cyclotron echoes detected by MARSIS may appear to be similar to the Bernstein mode waves detected by terrestrial ionospheric sounders, we do not believe that they are due to the excitation of Bernstein mode waves. The reason is that the electron cyclotron frequency in the ionosphere of Mars is typically a factor of one hundred, or more, below the transmitter frequency. Instead, we believe that the echoes are caused by the periodic return of electrons accelerated by the large voltages, typically several hundred volts, applied to the electric antenna during each cycle of the sounder pulse. Once accelerated, these electrons orbit in the local magnetic field where, as illustrated in Fig. 15, they periodically return to the vicinity of the antenna, thereby inducing a series of short broadband voltage pulses on the antenna at the electron cyclotron frequency. The impulsive character of these voltage signals accounts for the broadband (bar-shaped) response in the ionogram. Also, the explanation is consistent with the fact that the duration of the electron cyclotron echoes is always comparable to the duration of the transmitted pulse (91.3 μs), independent of the local magnetic field strength. For an energy of 100 eV and a magnetic field strength of 100 nT, which are typical values, the electron cyclotron radius is about 400 m. Since the cyclotron radius is considerably smaller than the typical scale size of the crustal magnetic fields, which is on the order of several hundred kilometers, the cyclotron period of electrons accelerated in different directions from the antenna would be nearly the same, which assures that they would return to the vicinity of the antenna at almost the same time, thereby providing a coherent response.

Since the Mars Express spacecraft does not have a magnetometer, electron cyclotron echoes provide a new and potentially useful method of measuring the local magnetic field. By scaling the time delay between the echoes from the ionogram, the magnetic field strength can be measured very accurately, typically about 1–3%. The main limitations are that the echoes not be so close together that they cannot be resolved (i.e., less than the 91.4 μs duration of the transmitter pulse) or so far apart that they fall outside of the
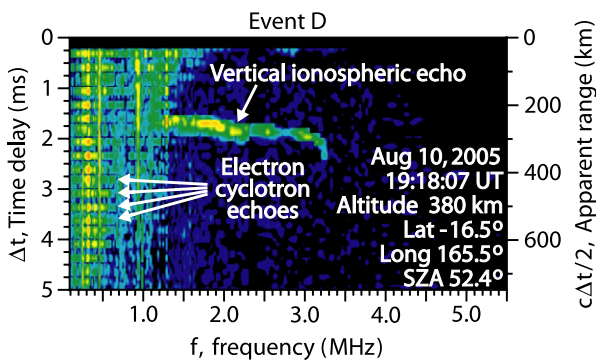

Fig. 14. An ionogram from the dayside of Mars that shows a series of electron cyclotron echoes in a region with a relatively strong crustal magnetic field. The electron cyclotron echoes appear as a series of horizontal bars, equally spaced in time, along the left-hand side of the ionogram. The inverse of the time spacing between these echoes is the local electron cyclotron frequency.
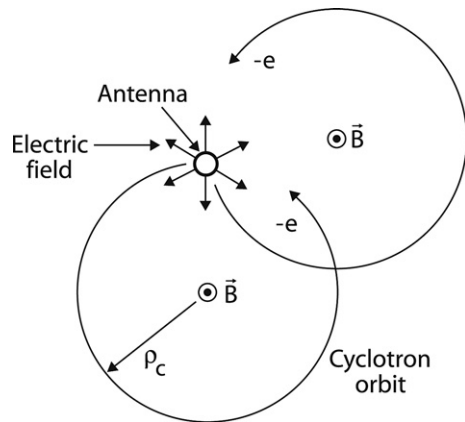
Fig. 15. An illustration of the mechanism by which the electron cyclotron echoes are believed to be produced. The small open circle is the cross-section of the electric dipole as viewed looking along the axis of the dipole. During the transmitter pulse electrons are accelerated by the large electric fields, several hundred V/m, in the vicinity of the antenna. Once accelerated the electrons orbit in the ambient magnetic field and return to the vicinity of the antenna every orbit, thereby inducing a series of broadband voltage pulses on the antenna. These pulses produce the horizontal bars in the ionogram (see Fig. 14).
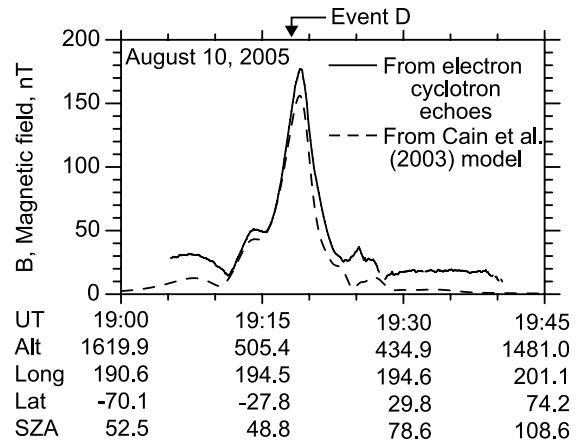

Fig. 16. A comparison of the magnetic field strength (solid line) computed from the electron cyclotron echoes with the magnetic field strength (dashed line) computed from the Cain et al. (2003) model for the pass from which the ionogram in Fig. 14 was selected. The small 20–30 nT discrepancy between the measured magnetic fields and the Cain et al. model is believed to be due to electrical currents flowing in the dayside ionopause.

7.31 ms window during which the echo intensities are sampled. To illustrate the type of magnetic field measurements that can be obtained using this technique, Fig. 16 shows a plot of the magnetic field strength computed from the electron cyclotron echoes observed during the pass from which the ionogram in Fig. 14 was selected. As can be seen, a very strong crustal magnetic field was encountered during this pass, reaching a peak of 180 nT at about 19:19 UT. For comparison the magnetic field strength computed from the Cain et al. (2003) model is shown by the dashed line. It is apparent that the magnetic field strength computed from the cyclotron echoes follows the field strength computed from the Cain et al. model very well. However, note that the measured magnetic field strength is generally about 20–30 nT greater than the field strength computed from the Cain et al. model. We believe that this small discrepancy has a simple explanation. The Cain et al. model is based on MGS magnetic field measurements which, because of technical limitations, can only be obtained from the nightside of Mars (Acuña et al., 1998). On the other hand the magnetic field measurements from the electron cyclotron echoes in Fig. 16 are mainly from the dayside of Mars. Because of electrical currents that flow in the dayside ionopause, the magnetic field strength in the ionosphere on the dayside of Mars is expected to be stronger than on the nightside. Although further study is necessary to confirm this interpretation, the magnetic field strength needed to provide pressure balance in the dayside ionosphere, 30–40 nT, given by Hanson and Mantas (1988), is in reasonable agreement with the 20–30 nT difference that we observed between the dayside magnetic field strength measurements obtained from the cyclotron echoes and the nightside crustal magnetic field strengths given by the Cain et al. model.

7. Summary

The ionospheric soundings obtained by MARSIS from the first year of in orbit operation around Mars have made important contributions to our knowledge of the Martian ionosphere. The vertical soundings of the ionosphere on the dayside of Mars show that the electron density in the main ionospheric layer is in reasonable agreement with the Chapman (1931) photo-equilibrium theory of planetary ionospheres. These soundings also show the possible presence of a second layer in the topside ionosphere at an altitude of about 200 km that is probably associated with O^+ ions. Oblique ionospheric echoes are also found to be a common feature of the MARSIS ionospheric soundings on the dayside of Mars. These echoes originate from density bulges in regions where the crustal magnetic field is nearly vertical. Detailed analyses and comparison with the MGS magnetic field data show that the density bulges have a horizontally elongated cylindrical structure, and that they tend to occur between oppositely directed arch-like magnetic field structures in the crustal magnetic field. It is believed that the density bulges are caused by solar wind electrons that have access to the lower levels of the ionosphere along nearly vertical open magnetic field lines. The resultant electron heating increases the plasma scale height and electron density of the ionosphere in these regions, thereby accounting for the density bulges. Several unusual ionospheric soundings were also discussed. These include observations of localized regions of very high density, possibly associated with plasma trapped in mini-magnetospheres or cusp-like magnetic field configurations formed by the strong crustal magnetic fields, and observations of diffuse echoes from density enhancements on the nightside of Mars, possibly associated with auroral electron precipitation. A new technique for measuring mag-

netic field strengths based on electron cyclotron echoes was also discussed. Comparisons of these magnetic field strengths with the fields computed from the Cain et al. (2003) model may provide a method of estimating the magnetic field contributed by currents flowing in the ionopause on the dayside of Mars.

Acknowledgments

References

Acuña, M.H., Connerney, J.E.P., Wasilewski, P., et al. Magnetic field and plasma observations at Mars: initial results of the Mars global surveyor mission. Science 279, 1676–1680, 1998.

Acuña, M.H., Connerney, J.E.P., Ness, N.F., et al. Global distribution of crustal magnetization discovered by the Mars global surveyor MAG/ER experiment. Science 284, 790–793, 1999.

Brace, L.H., Taulor Jr., H.A., Gombosi, et al. The ionosphere of Venus: observations and their interpretation, in: Hunten, D.M., Colin, L., Donahue, T.M., Moroz, V.I. (Eds.), Venus. University Arizona Press, Tucson, AZ, pp. 779–840, 1983.

Brain, D.A., Halekas, J.S., Peticolas, L.M., et al. On the origin of aurorae on Mars. Geophys. Res. Lett. 33, L01201, doi:10.1029/2005GL024782, 2006.

Budden, K.G. Radio Waves in the Ionosphere. Cambridge University Press, Cambridge, pp. 160–162, 1961.

Calvert, W. Ionospheric topside sounding. Science 154, 228–234, 1966.

Cain, J.C., Ferguson, B.B., Mozzoni, D. An $n = 90$ internal potential function of the martian crustal magnetic field. J. Geophys. Res. 108 (E2), 5008, doi:10.1029/2000JE001487, 2003.

Chapman, S. The absorption and dissociative or ionizing effect of monochromatic radiation in an atmosphere on a rotating Earth, Part II. Grazing incidence. Proc. Roy. Soc. London 43 (26), 483–501, 1931.

Chicarro, A., Martin, P., Traunter, R. The Mars Express mission: an overview, in: Wilson, A. (Ed.), Mars Express: a European Mission to the Red Planet, SP-1240. European Space Agency Publication Division, Noordwijk, Netherlands, pp. 3–16, 2004.

Connerney, J.E.P., Acuña, M.H., Ness, N.F., et al. Tectonic implications of Mars crustal magnetism. Proc. Natl. Acad. Sci. 102, 14970–14975, 2005.

Duru, F., Gurnett, D.A., Averkamp, T.F., et al. Magnetically controlled structures in the ionosphere of Mars. J. Geophys. Res. 111, A12204, doi:10.1029/2006JA011975, 2006.

Fjeldbo, G., Fjeldbo, W.C., Eshleman, V.R. Models for the atmosphere of Mars based on the Mariner 4 occultation experiment. J. Geophys. Res. 71, 2307–2316, 1966.

Fox, J.L. Upper limits to the outflow of ions at Mars. Geophys. Res. Lett. 24, 2901–2904, 1997.

Fox, J.L., Yeager, K.E. Morphology of the near-terminator Martian ionosphere: a comparison of models and data. J. Geophys. Res. 111, A10309, doi:1029/2006JA011697, 2006.

Franklin, C.A., Maclean, M.A. The design of swept-frequency topside sounders. Proc. IEEE 57, 897–944, 1969.

Gurnett, D.A., Bhattacharjee, A. Introduction to Plasma Physics with Space and Laboratory Applications. Cambridge University Press, Cambridge, p. 91, 2005.

Gurnett, D.A., Kirchner, D.L., Huff, R.L., et al. Radar soundings of the ionosphere of Mars. Science 310, 1929–1933, 2005.

Hagg, E.L., Hewens, E.J., Nelms, G.L. The interpretation of topside sounder ionograms. Proc. IEEE 57, 949–960, 1969.

Hanson, W.B., Sanatani, S., Zuccaro, D.R. The martian ionosphere as observed by the Viking retarding potential analyzers. J. Geophys. Res. 82, 4351–4363, 1977.

Hanson, W.B., Mantas, G.P. Viking electron temperature measurements: evidence for a magnetic field in the Martian ionosphere. J. Geophys. Res. 93, 7538–7544, 1988.

Kliore, A.J. Radio occultation observations of the ionospheres of Mar and Venus, in: Luhmann, J.G., Tatrallyay, M., Pepin, R. (Eds.), Venus and Mars, Ionospheres, and Solar Wind Interactions, Geophysics Monograph Series, vol. 66, pp. 265–276, 1992.

Krymskii, A.M., Breus, T.K., Ness, N.F., et al. Effect of crustal magnetic fields on the near terminator ionosphere at Mars: comparison of in situ magnetic field measurements with the data of radio science experiments on board Mars global surveyor. J. Geophys. Rev. 108 (A12), 1431, doi:10.1029/2002JA009662, 2003.

Krymskii, A.M., Ness, N.F., Crider, D.H., et al. Solar wind interaction with the ionosphere/atmosphere and crustal magnetic fields at Mars: Mars global surveyor magnetometer/electron reflectometer, radio science, and accelerometer data. J. Geophys. Res. 109, A11306, doi:1029/2004JA010420, 2004.

Luhmann, J.G., Brace, L.H. Near-Mars space. Rev. Geophys. 29, 121–140, 1991.

Lundin, R., Winningham, D., Barabash, S., et al. Plasma acceleration above Martian magnetic anomalies. Science 311 (5763), 980–983, doi:10.1126/science.1122071, 2006.

Ma, Y., Nagy, A.F., Sokolov, I.V., Hansen, K.C. Three-dimensional, multispecies, high spatial resolution MHD studies of the solar wind interaction with Mars. J. Geophys. Res. 109, A07211, doi:10.1029/2003JA010367, 2004.

Mendillo, M., Pi, X., Smith, S., et al. Ionospheric effects upon a satellite navigation system at Mars. Radio Sci. 39, RS2028, doi:10.1029/2003RS002933, 2004.

Mitchell, D.L., Lin, R.P., Mazelle, C., et al. Probing Mars' crustal magnetic field and ionosphere with the MGS electron reflectometer. J. Geophys. Res. 106, 23419–23428, 2001.

Morgan, D.D., Gurnett, D.A., Kirchner, D.L., et al. Solar control of radar wave absorption by the Martian ionosphere. Geophys. Res. Lett. 33, L13202, doi:10.1029/2006GL026637, 2006.

Ness, N.F., Acuña, M.H., Connerney, J.E.P., et al. Effects of magnetic anomalies discovered at Mars on the structure of the martian ionosphere and solar wind interaction as follows from radio occultation experiments. J. Geophys. Res. 105, 15991–16004, 2000.

Pätzold, M., Tellmann, S., Häusler, B., et al. A sporadic third layer in the ionosphere of Mars. Science 310, 837–839, 2005.

Picardi, G., Biccari, D., Seu, R., et al. MARSIS: Mars advanced radar for subsurface and ionosphere sounding, in: Wilson, A. (Ed.), Mars Express: a European mission to the red planet, SP-1240. European Space Agency Publication Division, Noordwijk, Netherlands, pp. 51–70, 2004.

Whittaker, E.T., Watson, G.N. A Cousre of Modern Analysis, fourth ed. Cambridge University Press, England, p. 229, 1927.

Shinagawa, H., Kim, J., Nagy, A.F., Cravens, T.E. A comprehensive magnetohydrodynamic model of the Venus ionosphere. J. Geophys. Res. 96, 11083–11095, 1991.

Wright, J.W., Argo, P.E., Pitteway, M.L.V. On the radiophysics and geophysics of ionogram spread F. Radio Sci. 31, 349–366, 1996.

Zhang, M.H.G., Luhmann, J.G., Kliore, A.J. A post pioneer Venus reassessment of the martian dayside ionosphere as observed by radar occultation methods. J. Geophys. Res. 95, 14829–14839, 1990a.

Zhang, M.G.H., Luhmann, J.G., Kliore, A.J. An observational study of the nightside ionosphere of Mars and Venus with radio occultation methods. J. Geophys. Res. 95, 17095–17102, 1990b.